

# SIRR-LMM: Single-image Reflection Removal via Large Multimodal Model

Yu Guo, Zhiqiang Lao, Xiyun Song, Yubin Zhou and Heather Yu  
 Futurewei Technologies, US  
 {yguo1, zlao, xsong, yzhou2, hyu}@futurewei.com

## Abstract

*Glass surfaces create complex interactions of reflected and transmitted light, making single-image reflection removal (SIRR) challenging. Existing datasets suffer from limited physical realism in synthetic data or insufficient scale in real captures. We introduce a synthetic dataset generation framework that path-traces 3D glass models over real background imagery to create physically accurate reflection scenarios with varied glass properties, camera settings, and post-processing effects. To leverage the capabilities of Large Multimodal Model (LMM), we concatenate the image layers into a single composite input, apply joint captioning, and fine-tune the model using task-specific LoRA rather than full-parameter training. This enables our approach to achieve improved reflection removal and separation performance compared to state-of-the-art methods.*

## 1. Introduction

Glass surfaces are common in everyday environments, appearing as windows, doors, picture frames, and display cases, *etc.* They introduce complex interactions between reflected and transmitted light, making accurate reflection removal or separation essential for applications such as photo retouching, autonomous driving, augmented reality, and digital heritage preservation.

Single-image reflection removal (SIRR) is inherently ill-posed because reflections and transmissions are tightly coupled, especially in over exposed regions. Real-world conditions further complicate the task through diverse lighting, scene geometry, and glass properties such as thickness or color, which limiting the effectiveness of classical decomposition methods.

Deep learning methods have made significant progress in SIRR through the use of sophisticated neural architectures and large-scale training. Recent advances in Large Multimodal Models (LMMs) further demonstrate strong capabilities in understanding and manipulating complex visual phenomena through text-based interactions. Since these foundation models are trained on billions of real-world images,

they naturally acquire prior knowledge about transparent materials, including glass. This makes them promising candidates for reflection removal, especially when a pre-trained general purpose model is further fine-tuned on a smaller dataset tailored to this task.

Despite these advantages, a major bottleneck in advancing reflection removal is the limited availability of high-quality training data. Real-world data collection is hindered by the difficulty of capturing accurate ground truth to separate reflection and transmission, while traditional synthetic datasets that simply blend two images fail to capture the physical realism needed for effective learning. These challenges restrict the development of more robust and reliable reflection removal systems.

We address this gap with a path-traced synthetic dataset that uses physically accurate 3D glass models combined with real background imagery. Our rendering pipeline simulates diverse glass and camera conditions using High Dynamic Range (HDR) environment maps for lighting and RGB images for near-field content. Instead of relying on large datasets, we fine-tune an LMM with task-specific Low-Rank Adaptation (LoRA), enabling strong performance with relatively small but high-fidelity synthetic data. Our main contributions include:

- A physically accurate synthetic dataset generation framework using ray tracing and real-world imagery, with an efficient approach that combines HDR environment maps with RGB images to avoid complex 3D scene modeling.
- To the best of our knowledge, this is the first work to explore the fine-tuned Large Multimodal Models for single-image reflection removal task.
- Empirical validation showing that appropriately adapted LMM with our synthetic data achieves superior reflection removal performance compared to previous approaches.

## 2. Related Work

### 2.1. Reflection Removal and Separation

Most SIRR methods focus on reflection removal to obtain clean images that contain only transmission content [3, 10, 22, 28, 33–35, 37, 38, 41, 45–47, 49, 56, 57, 59–61].

In certain applications, such as environment estimation [12], reflection separation becomes equally important. Several works have demonstrated the ability to generate both reflection and transmission images simultaneously [5, 6, 8, 13, 16–18, 25, 27, 36, 39, 40, 55]. Compared to reflection removal, reflection recovery presents greater challenges due to the inherent blurring and ghosting effects caused by double reflections and out-of-focus phenomena, making accurate recovery significantly more difficult.

To overcome the limitations of single-image approaches, researchers have explored various multi-modal strategies. Some works utilize polarized images [24, 31, 48, 52], while others rely on additional flash images [4, 23, 26, 42]. Alternative approaches include processing image sequences [30], incorporating semantic information [29], using text descriptions [14, 58], utilizing selfie images [21], or employing interactive methods [7]. For a complete coverage of these approaches, see more details in recent surveys [1, 43, 51].

## 2.2. Existing Datasets

Real captured datasets are built by capturing images with reflections, then blocking transmission to obtain reflection-only images, or removing reflective surface to produce clean transmission images. Popular datasets include SIR<sup>2</sup> [36], Real [55], Nature [27], CDR [25], and RRW [60]. Although video-based capture with camera or glass movement enables rapid dataset collection, it sacrifices diversity and often fails to achieve complete separation of reflection and transmission, leaving residual reflections inconsistencies. It also fails with changes in motion or lighting, making the resulting data unreliable for training.

Real data are often insufficient for comprehensive training, making synthetic data a necessary complement. A common strategy synthesizes reflections by mixing two tone-mapped images, typically expressed as  $I = f(T) + g(R)$  or  $I = f(T, R)$ , using datasets such as PASCAL VOC [9]. However, these approaches rely on simplified reflection models that do not capture real glass behavior. To address this, Kim *et al.* [22] estimate scene geometry from RGBD inputs and use path tracing to simulate light transport between scene meshes and glass. Since tone-mapped images do not preserve the true relationship between pixel values and scene luminance, Kee *et al.* [21] instead mixes linear RAW photos to construct more faithful data.

With these insights, our work integrates HDR environment maps with path tracing to generate synthetic data that better represent the lighting and reflection in the real-world. In addition, our method can easily extend to the non-planar surface, such as prescription eyeglasses [53].

## 2.3. Image synthesis LMM conditioned on text

Diffusion Transformers (DiT) [32] represent a major advancement in generative modeling by combining trans-

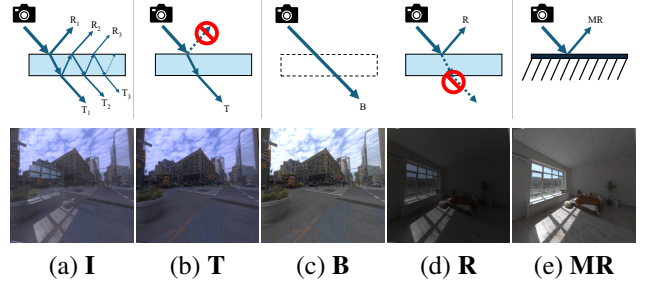


Figure 1. **Reflection and transmission.** (a) The Input image with glass reflection; (b) The Transmission component of **I**; (c) The Background image without glass; (d) The Reflection component of **I**; (e) The Mirror Reflection, which is considered as back scene image without any glass effects. We use blue tint glass to better illustrate the difference between **T** and **B**.

former architectures with diffusion processes. DiT uses self-attention to capture long-range dependencies and complex spatial relationships, enabling more sophisticated visual understanding and higher-quality image generation.

**FLUX.1 Kontext** [2] builds on the DiT to create a state-of-the-art generative model for complex visual manipulation tasks. Through Flow Matching training and context-aware processing, it can handle intricate phenomena such as glass reflections with high fidelity while providing precise and flexible control over the generation process.

**LoRA** [19] offers an efficient method for adapting large foundation models to specific tasks by adding low-rank matrices that encode task-specific behavior. This allows models like **FLUX.1 Kontext** to be customized for reflection removal using limited data while preserving their broad pre-trained knowledge.

We build our approach on **FLUX.1 Kontext** and train a LoRA specifically for our tasks.

## 3. Data Generation

Our dataset generation framework combines path-traced 3D glass models with real-world background imagery to create physically accurate reflection scenarios.

### 3.1. Path-traced scene setup

When light passes through glass, it generates effects such as blurring, ghosting, and attenuation. Image space synthesis methods must design appropriate degradation for reflection and transmission, which could involve using a weight, Gaussian, or even a trained network. Unlike previous synthetic methods, we simulate glass effects by physically modeling the glass and rendering it with path tracing [11]. The rendering equation for a non-emissive transparent surface point is,

$$L(\omega_o) = \int_{S^2} f(\omega_o, \omega) L(\omega) |\omega \cdot n| d\omega \quad (1)$$

where  $L$  is the radiance in the viewing direction  $\omega_o$ . The final rendering or pixel color is the result of integrating the

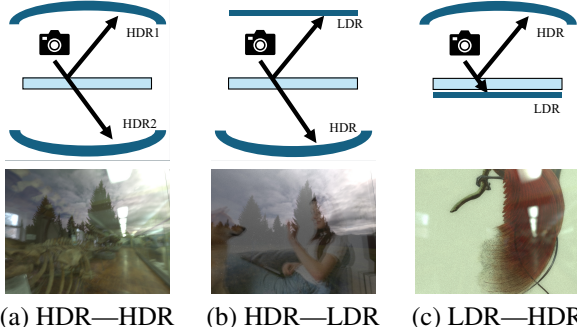


Figure 2. **Three different scenes setup.** (a) Use HDR environment maps for both transmission and reflection. (b) Use HDR map for transmission and put a LDR image behind camera for reflection. (c) Use HDR map for reflection and put a LDR image behind the glass for transmission.

energy from all light paths, weighted by the Bidirectional Reflectance Distribution Function (BRDF,  $f$ ) and the cosine of the angle between the normal surface ( $n$ ) and the direction of the light path ( $\omega$ ).

For a perfect glass slab, we can write down all the light paths (Figure 1-(a), top) by using  $\mathcal{T}$  (light hit glass and transmit/refract) and  $\mathcal{R}$  (light hit glass and reflect). All the transmissions,

$$T_1 + T_2 + T_3 + \dots = \mathcal{T}\mathcal{T} + \mathcal{T}\mathcal{R}^2\mathcal{T} + \mathcal{T}\mathcal{R}^4\mathcal{T} + \dots \quad (2)$$

and all the reflections,

$$R_1 + R_2 + R_3 + \dots = \mathcal{R} + \mathcal{T}\mathcal{R}\mathcal{T} + \mathcal{T}\mathcal{R}^3\mathcal{T} + \dots \quad (3)$$

For each  $\mathcal{T}$  and  $\mathcal{R}$ , the glass effects, such as blur or attenuation, contribute to the brightness of the image.

Figure 1 illustrates five rendered images and the illustration of their corresponding light paths.

- **I:** Input image with full glass effects.
- **T:** Transmission of the rendered glass with reflection disabled, showing the background.
- **B:** Background with the glass removed.
- **R:** Reflection part of the rendered glass with transmission disabled, displaying a dim scene reflection.
- **MR:** Mirror reflection, where changing the glass to a perfect mirror results in a sharp reflected scene.

The **I** contains both **T** ( $T_1 = \mathcal{T}\mathcal{T}$ ) and **R** ( $R_1 = \mathcal{R}$ ), as well as the higher-order ( $\mathcal{T}\mathcal{R}^k\mathcal{T}$ ) light interaction within the glass slab. **T** has typically been regarded as an estimate of **B**, until [24, 57] provided a detailed discourse. Compared to **B**, **T** is adding refraction shift and energy loss, which makes it look darker. Moreover, [22, 39] explicitly discusses the differences between **R** and **MR**. In short, **MR** has the same light path ( $\mathcal{R}$ ) as **R**, but with no energy loss. Our data generation pipeline is capable of producing all of these effects. **For the single-image reflection removal task, only I, T, and R are used.** However, the generated images retain broader potential, for instance, the pairs of **R** and **MR** can be applied to image enhancement tasks.

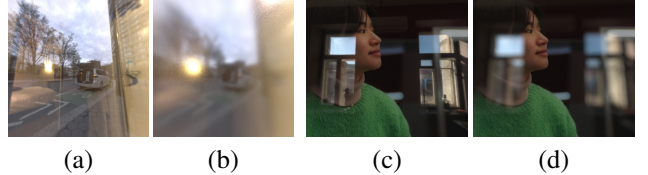


Figure 3. **Blurry effects.** (a) and (b): different roughness of the glass surface. (c) and (d): different aperture sizes of the camera.

In rendering images with glass effects, simply having the glass is insufficient; a complete 3D scene is necessary both in front of the glass (for reflections) and behind it (for transmissions). Creating such a 3D scene from scratch is complex and difficult to modify. As an alternative, [22] proposes estimating the depth from an RGB image to input into the renderer. However, this approach has a significant limitation: it cannot simulate light sources, which are crucial for tasks involving reflection removal. Consequently, highlights become overexposed and cannot be effectively simulated using LDR images. To address this, we used HDR environment maps to model the scene on both sides of the glass, as shown in Figure 2-(a).

To further enrich the dataset with scenarios that involve close proximity to glass, we introduce two additional scene configurations: I) since environment maps typically exclude humans or animals, we provide an alternative setup (Figure 2-(b)) that captures greater reflection variability, such as the frequent appearance of the photographer in the glass; II) Considering cases of photographing artwork behind protective glass, where reflections are concentrated within the frame while the artwork itself remains largely unaffected. As illustrated in Figure 2-(c), a scenario common in real-world settings such as museums and galleries, where reflective regions are ambiguous and can easily be mistaken for artwork content.

### 3.2. Scene parameter variation

To accurately represent the variety scenes in real-world applications, we parameterize several properties for glass. The thickness (residential windows could be 3 to 6 mm and structural/safety glass could be as thick as 10 to 40 mm), the color of the glass (from clear to diverse tints and color temperatures), the index of refraction (IOR) (from 1.45 to 1.65 to reflect different glass types), and the roughness of the surface (for the purpose of privacy, decoration, or light diffusion), see Figure 3-(a)(b). We also introduce double-layer glass (for thermal/sound insulation) by adding an additional glass layer and altering the interlayer distance. Double layers could generate the double reflection effect and also induce reflection, see Figure 4.

To ensure the dataset captures realistic imaging scenarios, we systematically vary camera parameters. Camera position is adjusted to provide multiple viewpoints relative to the glass surfaces, while the field of view is changed

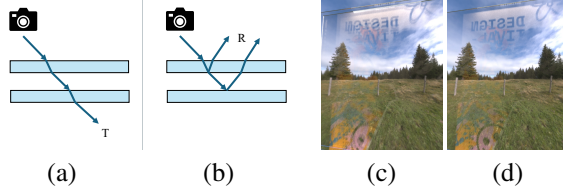


Figure 4. **Double reflection illustration.** (a) Transmission: turn off the reflection for both glass layers. (b) Reflection: only turn off the transmission for the bottom glass. (c) An example of double reflection. (d) A compared single reflection.

from wide-angle to telephoto perspectives. Focal distance and aperture size are also varied to produce different depth of field effects and defocus characteristics, further enhancing the diversity of the dataset, see Figure 3-(c)(d). Path-traced rendering is employed to guarantee physically accurate light transport. We use a sufficient number of ray bounces to capture complex light interactions, and adaptive sampling strategies are implemented for efficient rendering. The material models for glass surfaces are defined using physically-based BSDF to ensure that the rendered images closely match real-world observations.

To simulate real-world imaging conditions, we apply several post-processing effects to the rendered images. Gamma correction is performed using the standard sRGB curve, and auto white balance is applied to adjust the color temperature automatically. We also introduce JPEG compression artifacts to mimic the imperfections commonly found in digital photographs.

#### 4. Text-to-image Model Fine-tuning

Most of current text-to-image models, such as FLUX.1 Kontext model, could generate images conditioned jointly on a text prompt and a reference image. The conditional distribution is calculated as

$$p(x | y, c) \quad (4)$$

where  $x$  is target image,  $y$  is a condition image or guiding image, and  $c$  is a natural-language prompt.

Following the idea of In-Context LoRA [19], we generate the transmission and reflection components of a glare image simultaneously by directly concatenating them into a single large image  $[\mathbf{I}:\mathbf{T}:\mathbf{R}]$  during training (see **Output** in Figure 5), while consolidating their captions into a merged prompt with a high-level description for each panel. See **PROMPT** we used in Section 5.

The single consolidated prompt for the entire image set begins with an overall description, followed by individual prompts for each image. The correlations between the input image ( $\mathbf{I}$ ) and the decomposed images ( $\mathbf{T}$  and  $\mathbf{R}$ ) are implicitly maintained through the consolidated prompt. This unified prompt design is more compatible with existing text-to-image models and allows the overall description to naturally convey the task.

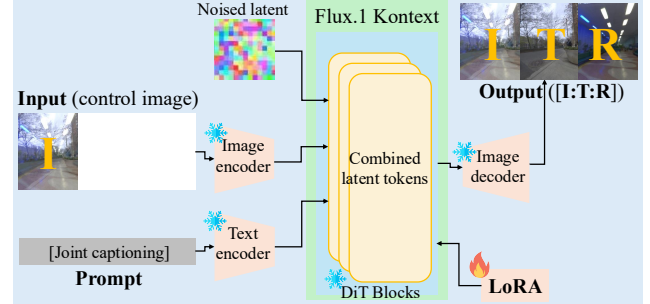


Figure 5. **Fine-tuning pipeline.** A overview of LoRA fine-tuning FLUX.1 Kontext with consolidated image pairs ( $[\mathbf{I}:\mathbf{T}:\mathbf{R}]$ ) and consolidated prompts.

Instead of providing different image sets with different prompts, we embed the prompt into the model as a feature specific to the task. In this way, the prompt does not need to be considered during inference, allowing our method to still be considered as a single-image reflection removal/separation. At the same time, we preserve the capability for in-context text-to-image generation to better handle the complex intrinsic relationships between each layer.

We keep the image  $\mathbf{I}$  both in both generated image and in the conditioning image to further enhance the correlation of the generated and conditioned images. We also reformulate this task to an image inpainting task by adding white space to the conditioning image (see **Input** in Figure 5), which is not necessary, but it turns out easier to converge.

#### 5. Experimental Setup

We provide a Python script to render the synthetic images. Each image set includes 5 JPEG images (see examples in Figure 13 from Appendix): the original rendered image with reflections, a ground truth transmission layer, a ground truth background image, a ground truth reflection layer, a ground truth mirror reflection image, and metadata describing the glass properties and camera parameters used in the rendering process. Original high dynamic linear images (.exr) are also provided. For HDR environment maps, we chose 140 indoor scenes and 30 outdoor nature scenes from Polyhaven<sup>1</sup>, and 110 outdoor city scenes from UrbanSky<sup>2</sup>. 200 high resolution LDR images are from the Internet with keyword searches, such as "human/pets" or "artwork".

With 1,000 image pairs rendered with our script, we build our approach on the FLUX.1 Kontext model and train an In-Context LoRA specifically for the task.  $\mathbf{T}$  and  $\mathbf{R}$  are concatenated into a single composite image,  $\mathbf{I}$  is used as control image, as we illustrated in 5. And captions for these images are fixed (see below **PROMPT**) during both training and inference, which makes it an internal parameter and does not offset the *single* image reflection removal rule.

<sup>1</sup><https://polyhaven.com/hdris>

<sup>2</sup><https://cave.cs.columbia.edu/repository/UrbanSky>

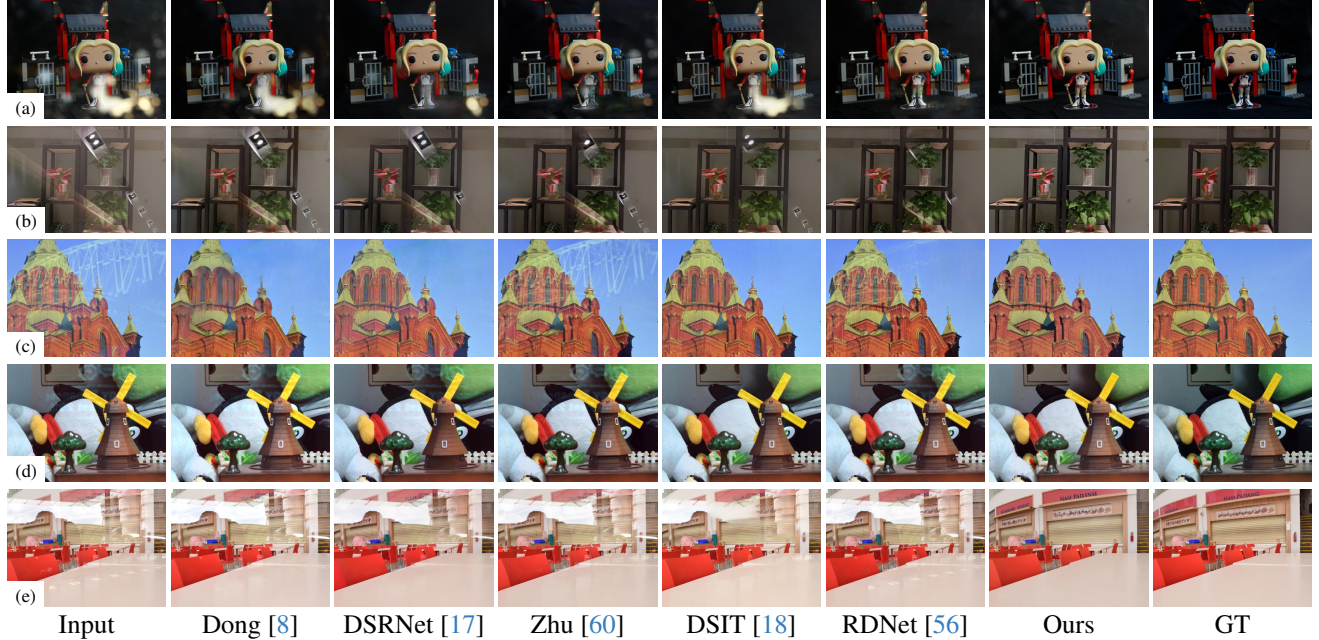


Figure 6. **Visual comparison of single-image reflection removal results.** The 5 examples are picking from *Real*, *Nature*, *SIR<sup>2</sup>-Postcard*, *SIR<sup>2</sup>-SolidObject* and *SIR<sup>2</sup>-Wild*. In general, our method could generate clean image and has a better prediction in the overexposed region.

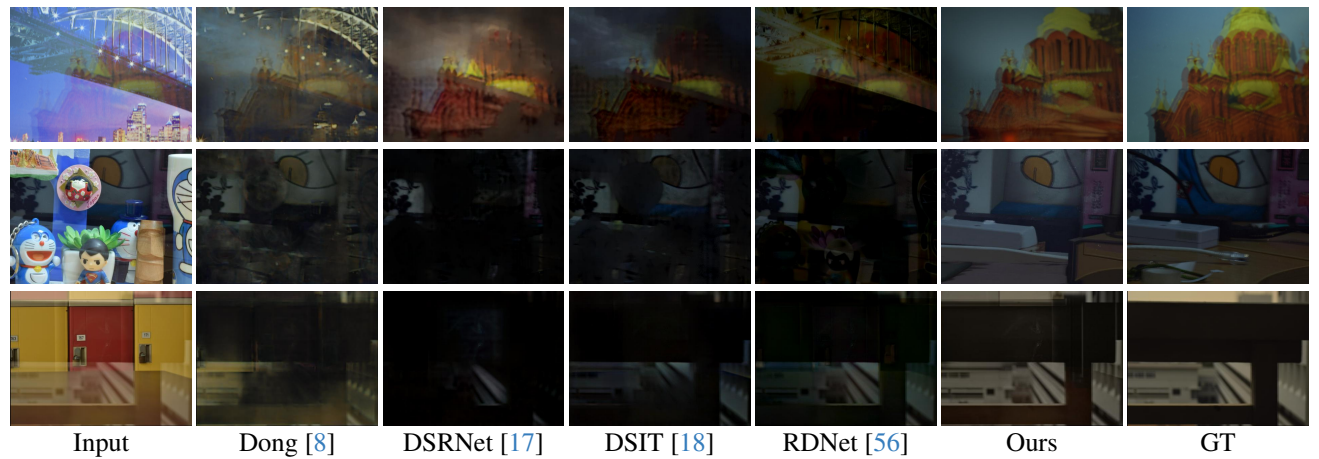


Figure 7. **Visual comparison of single-image reflection separation results.** The 3 examples are picking from *SIR<sup>2</sup>-Postcard*, *SIR<sup>2</sup>-SolidObject* and *SIR<sup>2</sup>-Wild*. Ours is the only method which could generate clean and meaningful reflection image.

#### PROMPT

This set of three images showcases an image decomposition task; [IMAGE1] captures an image looking through a transparent glass, both the scene behind the glass and the reflection of the glass could be seen; [IMAGE2] displays the transmission of glass with reflection removed; [IMAGE3] shows only the reflection of glass without transmission; [IMAGE1] could be decomposed to [IMAGE2] and [IMAGE3].

It is trained on a single 4090 GPU (24 G) for 4,000 steps with a batch size of 1 and a LoRA rank of 16. For inference, we employ 20 sampling steps with a guide scale of 4, which matches the distillation guide scale of FLUX.1 Kontext.

## 6. Results and Analysis

**The testing dataset.** Following prior work, we evaluate our fine-tuned LMM on three real-world reflection benchmarks: *Real* [55], *Nature* [27], and *SIR<sup>2</sup>* [36], which collectively cover diverse real-world reflection scenarios and are standard for assessing reflection removal performance. Note that there are 20 testing images in *Real* and 20 in *Nature*, while for *SIR<sup>2</sup>*, we tested 3 subcategories: for each scene setup in *Postcard*, there are 10 different glass/lens variances and we random choose one from each scene, and in total there are 20 images; we did the same to *SolidObject*; and we use all the 101 images in *Wildscene* as testing data.

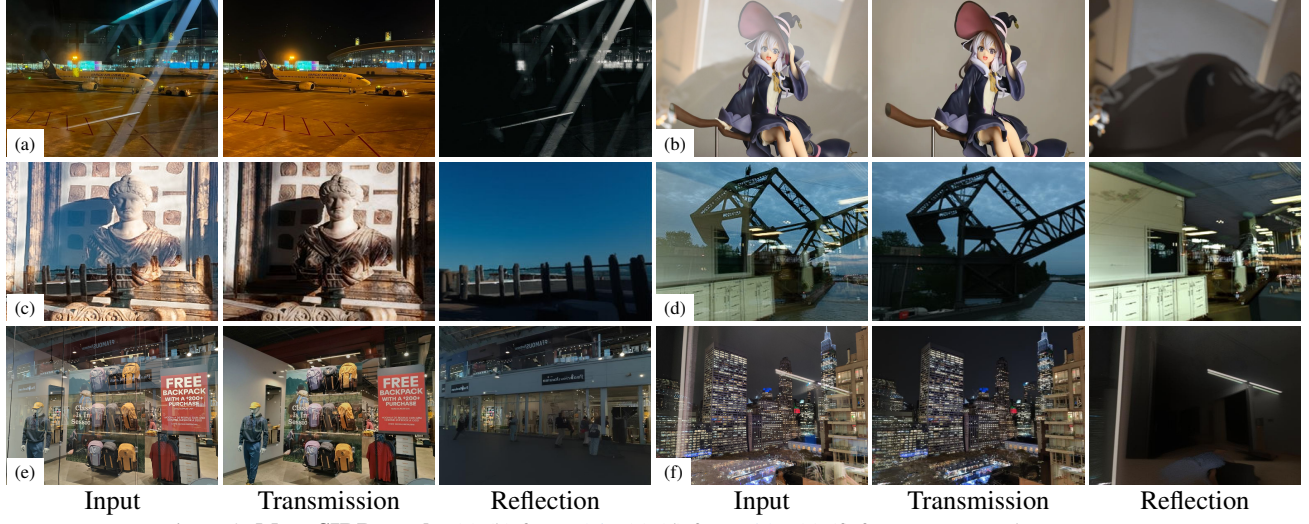


Figure 8. More SIRR results.(a) (b) from [15]; (c) (d) from [21]; (e) (f) from our smartphone captures.

Table 1. Quantitative comparisons on the real reflection benchmarks. The top-3 performing results are highlighted in **first**, second and **third**.  $P\uparrow$  is PSNR,  $S\uparrow$  is SSIM and  $L\downarrow$  is LPIPS. Ours (syn) is not ranked since it is the only one that does not include real training data. All the visual results in this paper are generated by Ours (syn).

| Method          | Real (20) [55] |              |                | Nature (20) [27] |              |                | SIR <sup>2</sup> (141) [36] |              |                |                  |              |                | Average (181)   |              |                |   |
|-----------------|----------------|--------------|----------------|------------------|--------------|----------------|-----------------------------|--------------|----------------|------------------|--------------|----------------|-----------------|--------------|----------------|---|
|                 |                |              |                |                  |              |                | Postcard (20)               |              |                | SolidObject (20) |              |                | Wildscene (101) |              |                |   |
|                 | P $\uparrow$   | S $\uparrow$ | L $\downarrow$ | P $\uparrow$     | S $\uparrow$ | L $\downarrow$ | P $\uparrow$                | S $\uparrow$ | L $\downarrow$ | P $\uparrow$     | S $\uparrow$ | L $\downarrow$ | P $\uparrow$    | S $\uparrow$ | L $\downarrow$ |   |
| Dong [8]        | 20.36          | 0.809        | 0.284          | 23.41            | 0.822        | 0.156          | 23.24                       | 0.882        | 0.165          | 23.87            | 0.909        | 0.093          | 23.97           | 0.914        | 0.109          | 23.418 0.8881 0.1380                      |
| DSRNet [17]     | 20.94          | 0.813        | 0.286          | 24.75            | 0.825        | 0.180          | 23.65                       | 0.898        | 0.154          | <u>26.55</u>     | 0.931        | <u>0.074</u>   | 26.56           | 0.932        | 0.088          | 25.416 0.9032 0.1258                      |
| Zhu [60]        | 22.85          | 0.829        | 0.255          | <u>25.64</u>     | <u>0.835</u> | <u>0.157</u>   | 23.69                       | 0.865        | 0.200          | <b>26.79</b>     | <b>0.936</b> | 0.075          | <b>26.88</b>    | 0.929        | 0.089          | 25.935 0.9013 0.1256                      |
| DSIT [18]       | <u>23.82</u>   | <u>0.852</u> | <u>0.231</u>   | <b>26.07</b>     | 0.833        | 0.183          | <u>25.08</u>                | <u>0.909</u> | <u>0.147</u>   | 26.53            | 0.932        | 0.076          | <u>26.84</u>    | <b>0.937</b> | <b>0.075</b>   | <u>26.192</u> 0.9125 0.1122               |
| RDNet [56]      | 24.22          | <b>0.859</b> | 0.228          | 25.78            | 0.838        | <u>0.171</u>   | <u>25.06</u>                | <u>0.906</u> | 0.140          | 26.60            | 0.934        | <b>0.072</b>   | 26.80           | 0.934        | <u>0.081</u>   | <u>26.188</u> 0.9120 0.1127               |
| Ours (syn+real) | <b>24.89</b>   | <u>0.858</u> | <u>0.227</u>   | 25.14            | <b>0.845</b> | <b>0.124</b>   | <b>26.18</b>                | <b>0.925</b> | <b>0.100</b>   | 26.41            | <u>0.933</u> | 0.073          | 26.86           | <u>0.933</u> | 0.076          | <b>26.327</b> <b>0.9141</b> <b>0.1003</b> |
| Ours (syn)      | 24.20          | 0.847        | 0.245          | 24.81            | 0.844        | 0.135          | 26.20                       | 0.933        | 0.099          | 26.34            | 0.931        | 0.072          | 26.85           | 0.932        | 0.078          | 26.204 0.9129 0.1044                      |

**Comparison methods.** Five most recent representative single-image reflection removal methods, Dong [8], DSRNet [17], Zhu [60], DSIT [18] and RDNet [56], are compared with our method. All methods could predict both **T** and **R** except Zhu. DSIT is based on the Vision Transformers structure, and RDNet wins the NTIRE 2025 single-image reflection removal in the wild challenge [50]. Both of them are considered state-of-the-art methods.

**Evaluation indicators.** We use PSNR [20] and SSIM [44] as error indicators following previous methods, and further adopt LPIPS [54] to measure the perceptual quality of the predicted results. Evaluations are performed using the same test scripts and the same testing data to ensure fairness.

## 6.1. Quantitative Performance

For all quantitative comparisons, we use the authors' official code and publicly released pre-trained weights without modification. To align with previous work, 289 image pairs from *Real* (89) and *Nature* (200) are added to the training

Table 2. Regional LPIPS ( $\downarrow$ ) on the reflection area.

| Method | Real         | Nature       | Postcard     | SolidObject  | Wildscene    | Average      |
|--------|--------------|--------------|--------------|--------------|--------------|--------------|
| DSIT   | 0.310        | 0.195        | 0.206        | 0.121        | 0.124        | 0.161        |
| RDNet  | <b>0.286</b> | 0.191        | 0.199        | 0.122        | 0.134        | 0.163        |
| Ours   | 0.299        | <b>0.186</b> | <b>0.110</b> | <b>0.102</b> | <b>0.107</b> | <b>0.137</b> |

data for quantitative comparisons. LoRA training takes 4 to 5 hours, and different training and testing image ratios and resolutions are supported.

Table 1 shows that our approach outperforms most competing methods across all test datasets. Given the diverse scenes, lightings in these real-world datasets, achieving consistently top results on all metrics is challenging. However, with only a small amount of high-quality synthetic data and reduced training time, our method still achieves performance comparable to leading techniques.

In many images, reflections occupy only a small portion, making the LPIPS score over the entire image less indicative of perceptual quality. To better capture our im-

Table 3. **User study comparison.** The win rate of our method, the tie rate and RDNet/DSIT win rate.

| Dataset     | Ours   | Tie    | RDNet  | Ours   | Tie    | DSIT   |
|-------------|--------|--------|--------|--------|--------|--------|
| Real        | 49.38% | 21.25% | 29.37% | 57.32% | 21.50% | 21.18% |
| Nature      | 35.00% | 42.08% | 22.92% | 35.00% | 53.75% | 11.25% |
| Postcard    | 55.37% | 18.66% | 25.97% | 67.03% | 12.26% | 20.71% |
| SolidObject | 41.43% | 26.96% | 31.61% | 40.37% | 26.06% | 33.57% |
| Wildscene   | 43.68% | 29.57% | 26.75% | 48.57% | 15.71% | 35.71% |
| Average     | 45.15% | 27.78% | 27.07% | 49.17% | 21.32% | 29.51% |

provement, we compute LPIPS only within the reflection regions, estimated from the difference between the input and reflection-free image. As shown in Table 2, our method yields an 18.2% improvement on reflection regions, compared to 7.7% when computed over the full image.

## 6.2. Qualitative Comparison

### 6.2.1. Single-image reflection removal

To further illustrate our advantages, Figure 6 presents visual comparisons of transmission layers against other methods. In example (a), while recent methods remove the out-of-focus highlights, only ours accurately inpaints the occluded area and correctly learns that the stand’s reflection should be red. Example (b) contains discontinuous reflections, where others achieve only partial removal, but our approach captures the full pattern. In examples (c) and (d), the watermark-like reflections make it difficult to distinguish reflection from transmission, yet our method produces clearer and more consistent results. For strong reflections, as in example (e), our method uniquely identifies the white region as reflection and generates plausible context for the shop’s name. Overall, our outputs are visually cleaner with fewer residual artifacts.

### 6.2.2. Single-image reflection separation

In Figure 7, we compare reflection layers and show that our method reconstructs reflection scenes more accurately than existing approaches. Unlike trivial cases dominated by highlight reflections, our goal is to recover informative reflection content embedded in the image. According to Snell’s law, most optical energy is transmitted through glass, and reflections become prominent only at grazing incidence. Even under limited information and near-dark reflections, our method uniquely estimates the reflection across the entire image while plausibly synthesizing content in regions with extremely low visibility.

### 6.2.3. More results for real captured images

We observe that existing methods perform well on current benchmarks, suggesting possible overfitting to older datasets. To further assess practicality, we evaluate our approach on additional real-world reflection images. As shown in Figure 8, our method achieves an accurate separation of the reflection and transmission layers: the recovered



Figure 9. **The Comparison of our result with basic Flux model.** LMMs have the capability in reflection removal but often require carefully designed prompts. In contrast, our method leverages limited training data to enable non-specific image prompts.

transmission preserves fine details behind the glass, while the estimated reflection retains reflective elements within the frame. These results highlight the robustness of our method in complex real-world scenarios. See Figure 14 in Appendix for the full comparison results.

## 6.3. User Study

Although the similarity scores in Table 1 are close among our method, RDNet and DSIT, our results are often visually superior in reflection removal cleanliness, fewer artifacts and overall image quality. To validate, we conducted a user study with 100 participants. Each subject was randomly assigned 40 image pairs. For each pair, they were shown an input image with reflections and two outputs, ours and a comparison method, then asked to choose the better result or indicate “similar”. Our method achieved a 45.15% win rate (72.93% win+tie) against RDNet and 49.17% (70.49% win+tie) against DSIT, showing a clear subjective preference for our results. See Table 3 for more details.

## 6.4. Ablation Studies

### 6.4.1. Comparing to original Flux model

Compared to other text-to-image LMMs, FLUX.1 Kontext stands out as an open-source option with strong iterative editing capabilities and image quality. Same as other LMMs, it often struggles when using a fixed and generic prompt, requiring carefully tailored user input to achieve good results. In contrast, our fine-tuned model addresses this limitation by removing the dependency on user-specific prompts, consistently delivering effective edits from a constant input. See example in Figure 9.

### 6.4.2. Comparing to 8-bit mixture synthetic data

To further assess the quality of our synthetic data, we follow RDNet and generate comparison images by linearly blending 8-bit tone-mapped images using  $I = \alpha T + \beta R - T \circ R$ . As shown in Figure 10, we use identical transmission and reflection content in both methods to ensure a fair comparison. Prior approaches synthesize reflections by mixing 8-bit tone-mapped images, often producing brighter and “flatter” results: simulated reflections lack overexposed highlights

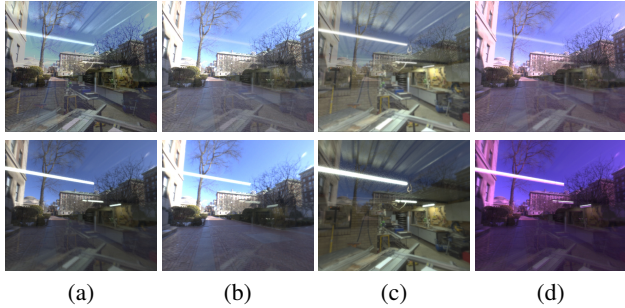


Figure 10. **The comparison of our synthetic data with the previous work.** The top row is the linear combination of two 8-bit LDR images that follow RDNet and the bottom row is generated using our synthesis method. The same transmission (outdoor) and reflection (indoor) scenes are used here for all the images. The top looks washed out and bottom has higher contrast which is more like a real photo.

Table 4. **LPIPS (↓) on different synthetic training data.** Ours is trained with our synthetic data; and Ours-RDNet is trained with the data generated using synthetic strategy from RDNet.

| Method     | Real  | Nature | Postcard | SolidObject | Wildscene | Average |
|------------|-------|--------|----------|-------------|-----------|---------|
| Ours       | 0.302 | 0.218  | 0.111    | 0.108       | 0.109     | 0.142   |
| Ours-RDNet | 0.316 | 0.227  | 0.112    | 0.140       | 0.131     | 0.161   |

and appear disproportionately strong in shadowed regions, lifting the black levels and creating a washed-out look. In real scenes, when the outdoor environment is bright, indoor illumination is weak and reflections appear only near lights or windows (Figure 10-(b)), whereas at dusk larger portions of the indoor scene may reflect onto the outdoor view (Figure 10-(c)). Zooming into the white fluorescent light strip in Figure 10-(d), the reflection is not a single sharp rectangle but shows a “shaky” double edge and a faint halo-artifacts of refraction and ghosting caused by real glass thickness.

To assess the impact of synthetic data quality on training, we generated 1000 image pairs using blending-based methods, kept the underlying scene fixed, and fine-tuned the Flux model. The resulting model consistently underperformed compared to training on our synthetic dataset. A detailed regional LPIPS comparison is shown in Table 4.

#### 6.4.3. Training size

To understand how training data size affects LoRA fine-tuning, we conduct an ablation study where the number of synthetic training pairs varies from 0 to 1000 (0 means no fine-tuning). As shown in Figure 11, the results reveal a clear and consistent trend across all metrics. Without training, performance is limited: SSIM stays below 0.81, PSNR is around 20 dB, and LPIPS remains high ( $>0.5$ ), indicating insufficient generalization, also evident in Figure 9. With 10–50 samples, all metrics improve sharply, PSNR increases by more than 4 dB and SSIM rises above 0.88, highlighting the strong data efficiency of LoRA when

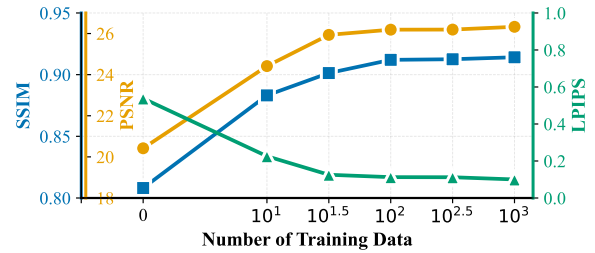


Figure 11. **Ablation on training data size for fine-tuning.** Performance improves rapidly with more samples and stabilizes after a few hundred.



Figure 12. **Failure cases.** The white logo (in the yellow box) is on the background but was incorrectly removed as a reflection; the white reflection (in the green box) is mistakenly kept because it is treated as part of the background.

adapting a pretrained LMM. Beyond roughly 300 samples, the gains taper off and the curves saturate, suggesting diminishing returns once the model has captured the task’s diversity. Overall, these findings show that while LoRA benefits from more data, a few hundred samples are sufficient for stable and competitive performance in SIRR.

## 7. Limitations

Although our approach provides substantial improvements, several limitations remain. Path-traced rendering, despite its high physical fidelity, requires considerable computational resources, which could only generate dataset offline. In addition, white background areas are occasionally misclassified as highlight reflections to be removed and vice versa. See Figure 12.

## 8. Conclusion

We have presented a novel framework for generating physically accurate synthetic datasets for glass reflection removal. Our approach combines path-traced 3D glass models with real-world background imagery, providing a scalable solution for creating large-scale datasets with controlled parameterization. The evaluation using LoRA fine-tuning with Flux demonstrates the effectiveness of our synthetic data for real-world reflection removal tasks. Our work addresses the critical need for high-quality training data in glass reflection removal and provides a foundation for future research in this important area of computer vision.

## References

[1] Ali Amanlou, Amir Abolfazl Suratgar, Jafar Tavoosi, Ardashir Mohammadzadeh, and Amir Mosavi. Single-image reflection removal using deep learning: a systematic review. *IEEE Access*, 10:29937–29953, 2022. 2

[2] Stephen Batifol, Andreas Blattmann, Frederic Boesel, Saksham Consul, Cyril Diagne, Tim Dockhorn, Jack English, Zion English, Patrick Esser, Sumith Kulal, et al. Flux. 1 kontext: Flow matching for in-context image generation and editing in latent space. *arXiv e-prints*, pages arXiv–2506, 2025. 2

[3] Jie Cai, Kangning Yang, Ling Ouyang, Lan Fu, Jiaming Ding, Huiming Sun, Chiu Man Ho, and Zibo Meng. F2t2-bit: A u-shaped fft transformer and hierarchical transformer for reflection removal. *arXiv preprint arXiv:2506.05489*, 2025. 1

[4] Yakun Chang, Cheolkon Jung, Jun Sun, and Fengqiao Wang. Siamese dense network for reflection removal with flash and no-flash image pairs. *International Journal of Computer Vision*, 128(6):1673–1698, 2020. 2

[5] Ya-Chu Chang, Chia-Ni Lu, Chia-Chi Cheng, and Wei-Chen Chiu. Single image reflection removal with edge guidance, reflection classifier, and recurrent decomposition. In *Proceedings of the IEEE/CVF winter conference on applications of computer vision*, pages 2033–2042, 2021. 2

[6] Songnan Chen and Zhaoxu Feng. High-resolution image reflection removal by laplacian-based component-aware transformer. *Scientific Reports*, 15(1):9972, 2025. 2

[7] Xiao Chen, Xudong Jiang, Yunkang Tao, Zhen Lei, Qing Li, Chenyang Lei, and Zhaoxiang Zhang. Firm: Flexible interactive reflection removal. In *Proceedings of the AAAI Conference on Artificial Intelligence*, pages 2230–2238, 2025. 2

[8] Zheng Dong, Ke Xu, Yin Yang, Hujun Bao, Weiwei Xu, and Rynson WH Lau. Location-aware single image reflection removal. In *Proceedings of the IEEE/CVF international conference on computer vision*, pages 5017–5026, 2021. 2, 5, 6, 12

[9] Mark Everingham, Luc Van Gool, Christopher KI Williams, John Winn, and Andrew Zisserman. The pascal visual object classes (voc) challenge. *International journal of computer vision*, 88(2):303–338, 2010. 2

[10] Qingnan Fan, Jiaolong Yang, Gang Hua, Baoquan Chen, and David Wipf. A generic deep architecture for single image reflection removal and image smoothing. In *Proceedings of the IEEE International Conference on Computer Vision*, pages 3238–3247, 2017. 1

[11] Yu Guo, Miloš Hašan, and Shuang Zhao. Position-free Monte Carlo simulation for arbitrary layered BSDFs. *ACM Transactions on Graphics (ToG)*, 37(6):1–14, 2018. 2

[12] Yu Guo, Zhiqiang Lao, Xiyun Song, Yubin Zhou, Zongfang Lin, and Heather Yu. ePBR: Extended PBR materials in image synthesis. In *Proceedings of the Computer Vision and Pattern Recognition Conference*, pages 327–336, 2025. 2

[13] Lingzhi He, Feng Li, Runmin Cong, and Yao Zhao. Reflection intensity guided single image reflection removal and transmission recovery. *IEEE Transactions on Multimedia*, 26:5026–5039, 2023. 2

[14] Yuchen Hong, Haofeng Zhong, Shuchen Weng, Jinxiu Liang, and Boxin Shi. L-differ: Single image reflection removal with language-based diffusion model. In *European Conference on Computer Vision*, pages 58–76. Springer, 2024. 2

[15] Jichen Hu, Chen Yang, Zanwei Zhou, Jiemin Fang, Xiaokang Yang, Qi Tian, and Wei Shen. Derelection any image with diffusion priors and diversified data. *arXiv preprint arXiv:2503.17347*, 2025. 6, 12

[16] Qiming Hu and Xiaojie Guo. Trash or treasure? an interactive dual-stream strategy for single image reflection separation. *Advances in Neural Information Processing Systems*, 34:24683–24694, 2021. 2

[17] Qiming Hu and Xiaojie Guo. Single image reflection separation via component synergy. In *Proceedings of the IEEE/CVF international conference on computer vision*, pages 13138–13147, 2023. 5, 6, 12

[18] Qiming Hu, Hainuo Wang, and Xiaojie Guo. Single image reflection separation via dual-stream interactive transformers. *Advances in Neural Information Processing Systems*, 37:55228–55248, 2024. 2, 5, 6, 12

[19] Lianghua Huang, Wei Wang, Zhi-Fan Wu, Yupeng Shi, Huanzhang Dou, Chen Liang, Yutong Feng, Yu Liu, and Jingen Zhou. In-context lora for diffusion transformers. *arXiv preprint arXiv:2410.23775*, 2024. 2, 4

[20] Quan Huynh-Thu and Mohammed Ghanbari. Scope of validity of psnr in image/video quality assessment. *Electronics letters*, 44(13):800–801, 2008. 6

[21] Eric Kee, Adam Pikielny, Kevin Blackburn-Matzen, and Marc Levoy. Removing reflections from raw photos. In *Proceedings of the Computer Vision and Pattern Recognition Conference*, pages 161–171, 2025. 2, 6, 12

[22] Soomin Kim, Yuchi Huo, and Sung-Eui Yoon. Single image reflection removal with physically-based training images. In *Proceedings of the IEEE/CVF conference on computer vision and pattern recognition*, pages 5164–5173, 2020. 1, 2, 3

[23] Chenyang Lei and Qifeng Chen. Robust reflection removal with reflection-free flash-only cues. In *Proceedings of the IEEE/CVF Conference on Computer Vision and Pattern Recognition*, pages 14811–14820, 2021. 2

[24] Chenyang Lei, Xuhua Huang, Mengdi Zhang, Qiong Yan, Wenxiu Sun, and Qifeng Chen. Polarized reflection removal with perfect alignment in the wild. In *Proceedings of the IEEE/CVF conference on computer vision and pattern recognition*, pages 1750–1758, 2020. 2, 3

[25] Chenyang Lei, Xuhua Huang, Chenyang Qi, Yankun Zhao, Wenxiu Sun, Qiong Yan, and Qifeng Chen. A categorized reflection removal dataset with diverse real-world scenes. In *Proceedings of the IEEE/CVF Conference on Computer Vision and Pattern Recognition*, pages 3040–3048, 2022. 2

[26] Chenyang Lei, Xudong Jiang, and Qifeng Chen. Robust reflection removal with flash-only cues in the wild. *IEEE Transactions on Pattern Analysis and Machine Intelligence*, 45(12):15530–15545, 2023. 2

[27] Chao Li, Yixiao Yang, Kun He, Stephen Lin, and John E Hopcroft. Single image reflection removal through cascaded

refinement. In *Proceedings of the IEEE/CVF conference on computer vision and pattern recognition*, pages 3565–3574, 2020. [2](#), [5](#), [6](#)

[28] Yu Li, Ming Liu, Yaling Yi, Qince Li, Dongwei Ren, and Wangmeng Zuo. Two-stage single image reflection removal with reflection-aware guidance. *Applied Intelligence*, 53(16):19433–19448, 2023. [1](#)

[29] Yunfei Liu, Yu Li, Shaodi You, and Feng Lu. Semantic guided single image reflection removal. *ACM Transactions on Multimedia Computing, Communications and Applications*, 18(3s):1–23, 2022. [2](#)

[30] Yu-Lun Liu, Wei-Sheng Lai, Ming-Hsuan Yang, Yung-Yu Chuang, and Jia-Bin Huang. Learning to see through obstructions. In *Proceedings of the IEEE/CVF Conference on Computer Vision and Pattern Recognition*, pages 14215–14224, 2020. [2](#)

[31] Youwei Lyu, Zhaopeng Cui, Si Li, Marc Pollefeys, and Boxin Shi. Reflection separation using a pair of unpolarized and polarized images. *Advances in neural information processing systems*, 32, 2019. [2](#)

[32] William Peebles and Saining Xie. Scalable diffusion models with transformers. In *Proceedings of the IEEE/CVF international conference on computer vision*, pages 4195–4205, 2023. [2](#)

[33] BH Prasad, Lokesh R Boregowda, Kaushik Mitra, Sanjoy Chowdhury, et al. V-desirr: Very fast deep embedded single image reflection removal. In *Proceedings of the IEEE/CVF International Conference on Computer Vision*, pages 2390–2399, 2021. [1](#)

[34] Green Rosh, Pawan Prasad B H, Lokesh R. Boregowda, and Kaushik Mitra. R2sfd: Improving single image reflection removal using semantic feature dictionary. In *Proceedings of the 32nd ACM International Conference on Multimedia*, page 10277–10286. Association for Computing Machinery, 2024.

[35] Zhenbo Song, Zhenyuan Zhang, Kaihao Zhang, Wenhan Luo, Zhaoxin Fan, Wenqi Ren, and Jianfeng Lu. Robust single image reflection removal against adversarial attacks. In *Proceedings of the IEEE/CVF conference on computer vision and pattern recognition*, pages 24688–24698, 2023. [1](#)

[36] Renjie Wan, Boxin Shi, Ling-Yu Duan, Ah-Hwee Tan, and Alex C Kot. Benchmarking single-image reflection removal algorithms. In *Proceedings of the IEEE international conference on computer vision*, pages 3922–3930, 2017. [2](#), [5](#), [6](#)

[37] Renjie Wan, Boxin Shi, Ling-Yu Duan, Ah-Hwee Tan, and Alex C Kot. Crrn: Multi-scale guided concurrent reflection removal network. In *Proceedings of the IEEE Conference on Computer Vision and Pattern Recognition*, pages 4777–4785, 2018. [1](#)

[38] Renjie Wan, Boxin Shi, Haoliang Li, Ling-Yu Duan, Ah-Hwee Tan, and Alex C Kot. Corrn: Cooperative reflection removal network. *IEEE transactions on pattern analysis and machine intelligence*, 42(12):2969–2982, 2019. [1](#)

[39] Renjie Wan, Boxin Shi, Haoliang Li, Ling-Yu Duan, and Alex C Kot. Reflection scene separation from a single image. In *Proceedings of the IEEE/CVF Conference on Computer Vision and Pattern Recognition*, pages 2398–2406, 2020. [2](#), [3](#)

[40] Renjie Wan, Boxin Shi, Haoliang Li, Yuchen Hong, Ling-Yu Duan, and Alex C Kot. Benchmarking single-image reflection removal algorithms. *IEEE Transactions on Pattern Analysis and Machine Intelligence*, 45(2):1424–1441, 2022. [2](#)

[41] Ce Wang, Dejia Xu, Renjie Wan, Bin He, Boxin Shi, and Ling-Yu Duan. Background scene recovery from an image looking through colored glass. *IEEE Transactions on Multimedia*, 25:2876–2887, 2022. [1](#)

[42] Tianfu Wang, Mingyang Xie, Haoming Cai, Sachin Shah, and Christopher A Metzler. Flash-split: 2d reflection removal with flash cues and latent diffusion separation. In *Proceedings of the Computer Vision and Pattern Recognition Conference*, pages 5688–5698, 2025. [2](#)

[43] Xin Wang, Yong Zhang, Junfeng Xu, and Jun Gao. A review on learning based image reflection removal algorithms. *Intelligent Data Analysis*, 29(1):5–27, 2025. [2](#)

[44] Zhou Wang, Eero P Simoncelli, and Alan C Bovik. Multi-scale structural similarity for image quality assessment. In *The thirty-seventh asilomar conference on signals, systems & computers, 2003*, pages 1398–1402. Ieee, 2003. [6](#)

[45] Ao Wei, Hanbin Zhang, and Erhu Zhao. Derelectformer: vision transformers for single image reflection removal. In *International conference on pattern recognition*, pages 257–274. Springer, 2024. [1](#)

[46] Kaixuan Wei, Jiaolong Yang, Ying Fu, David Wipf, and Hua Huang. Single image reflection removal exploiting misaligned training data and network enhancements. In *Proceedings of the IEEE/CVF Conference on Computer Vision and Pattern Recognition*, pages 8178–8187, 2019.

[47] Qiang Wen, Yinjie Tan, Jing Qin, Wenxi Liu, Guoqiang Han, and Shengfeng He. Single image reflection removal beyond linearity. In *Proceedings of the IEEE/CVF Conference on Computer Vision and Pattern Recognition*, pages 3771–3779, 2019. [1](#)

[48] Patrick Wieschollek, Orazio Gallo, Jinwei Gu, and Jan Kautz. Separating reflection and transmission images in the wild. In *Proceedings of the European Conference on Computer Vision (ECCV)*, pages 89–104, 2018. [2](#)

[49] Jie Yang, Dong Gong, Lingqiao Liu, and Qinfeng Shi. Seeing deeply and bidirectionally: A deep learning approach for single image reflection removal. In *Proceedings of the european conference on computer vision (ECCV)*, pages 654–669, 2018. [1](#)

[50] Kangning Yang, Jie Cai, Ling Ouyang, Florin-Alexandru Vasluiianu, Radu Timofte, Jiaming Ding, Huiming Sun, Lan Fu, Jinlong Li, Chiu Man Ho, et al. Ntire 2025 challenge on single image reflection removal in the wild: Datasets, methods and results. In *Proceedings of the Computer Vision and Pattern Recognition Conference*, pages 1301–1311, 2025. [6](#)

[51] Kangning Yang, Huiming Sun, Jie Cai, Lan Fu, Jiaming Ding, Jinlong Li, Chiu Man Ho, and Zibo Meng. Survey on single-image reflection removal using deep learning techniques. *arXiv preprint arXiv:2502.08836*, 2025. [2](#)

[52] Mingde Yao, Menglu Wang, King-Man Tam, Lingen Li, Tianfan Xue, and Jinwei Gu. Polarfree: Polarization-based

reflection-free imaging. In *Proceedings of the Computer Vision and Pattern Recognition Conference*, pages 10890–10899, 2025. 2

[53] Qian Zhang, Yu Guo, Pierre-Yves Laffont, Tobias Martin, and Markus Gross. A virtual try-on system for prescription eyeglasses. *IEEE computer graphics and applications*, 37(4):84–93, 2017. 2

[54] Richard Zhang, Phillip Isola, Alexei A Efros, Eli Shechtman, and Oliver Wang. The unreasonable effectiveness of deep features as a perceptual metric. In *Proceedings of the IEEE conference on computer vision and pattern recognition*, pages 586–595, 2018. 6

[55] Xuaner Zhang, Ren Ng, and Qifeng Chen. Single image reflection separation with perceptual losses. In *Proceedings of the IEEE conference on computer vision and pattern recognition*, pages 4786–4794, 2018. 2, 5, 6

[56] Hao Zhao, Mingjia Li, Qiming Hu, and Xiaojie Guo. Reversible decoupling network for single image reflection removal. In *Proceedings of the Computer Vision and Pattern Recognition Conference*, pages 26430–26439, 2025. 1, 5, 6, 12

[57] Qian Zheng, Boxin Shi, Jinnan Chen, Xudong Jiang, Ling-Yu Duan, and Alex C Kot. Single image reflection removal with absorption effect. In *Proceedings of the IEEE/CVF conference on computer vision and pattern recognition*, pages 13395–13404, 2021. 1, 3

[58] Haofeng Zhong, Yuchen Hong, Shuchen Weng, Jinxiu Liang, and Boxin Shi. Language-guided image reflection separation. In *Proceedings of the IEEE/CVF Conference on Computer Vision and Pattern Recognition*, pages 24913–24922, 2024. 2

[59] Yurui Zhu, Xueyang Fu, Zheyu Zhang, Aiping Liu, Zhiwei Xiong, and Zheng-Jun Zha. Hue guidance network for single image reflection removal. *IEEE transactions on neural networks and learning systems*, 35(10):13701–13712, 2023. 1

[60] Yurui Zhu, Xueyang Fu, Peng-Tao Jiang, Hao Zhang, Qibin Sun, Jinwei Chen, Zheng-Jun Zha, and Bo Li. Revisiting single image reflection removal in the wild. In *Proceedings of the IEEE/CVF Conference on Computer Vision and Pattern Recognition*, pages 25468–25478, 2024. 2, 5, 6, 12

[61] Zhengxia Zou, Sen Lei, Tianyang Shi, Zhenwei Shi, and Jieping Ye. Deep adversarial decomposition: A unified framework for separating superimposed images. In *Proceedings of the IEEE/CVF conference on computer vision and pattern recognition*, pages 12806–12816, 2020. 1

## Appendix

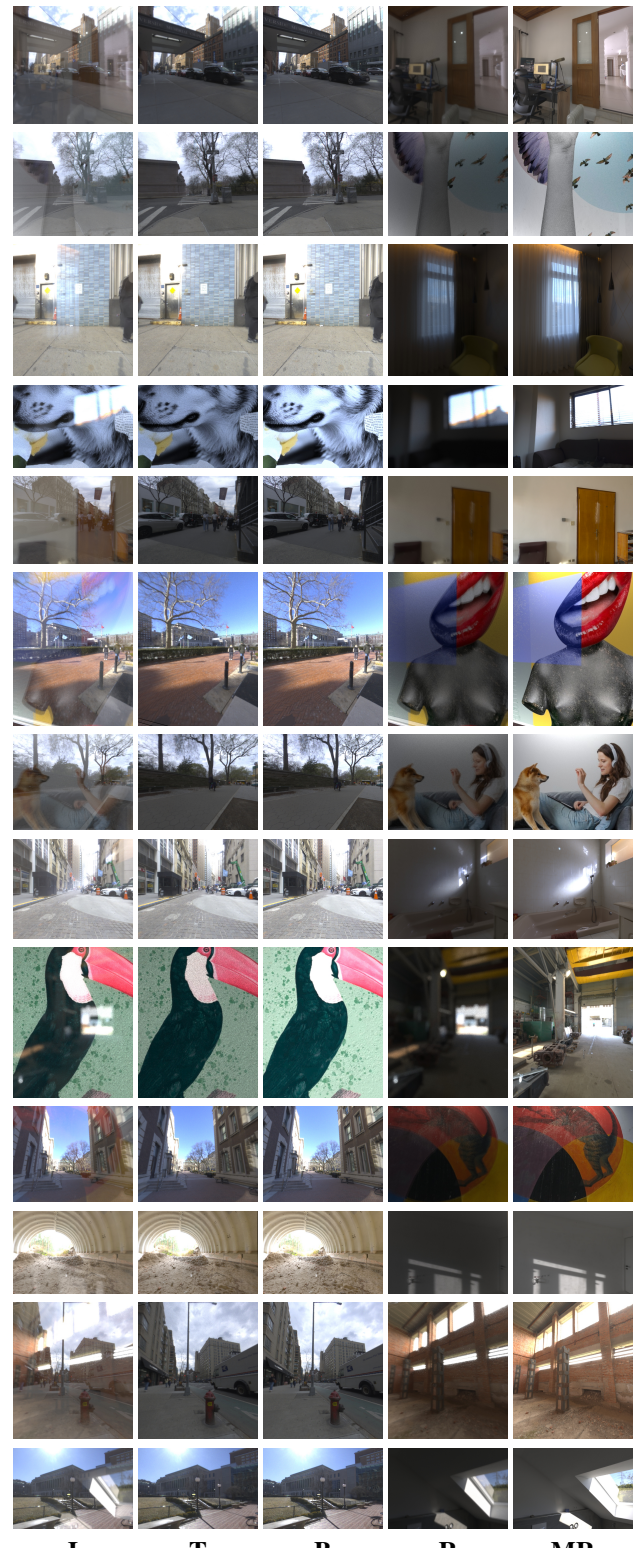


Figure 13. Our synthetic data examples

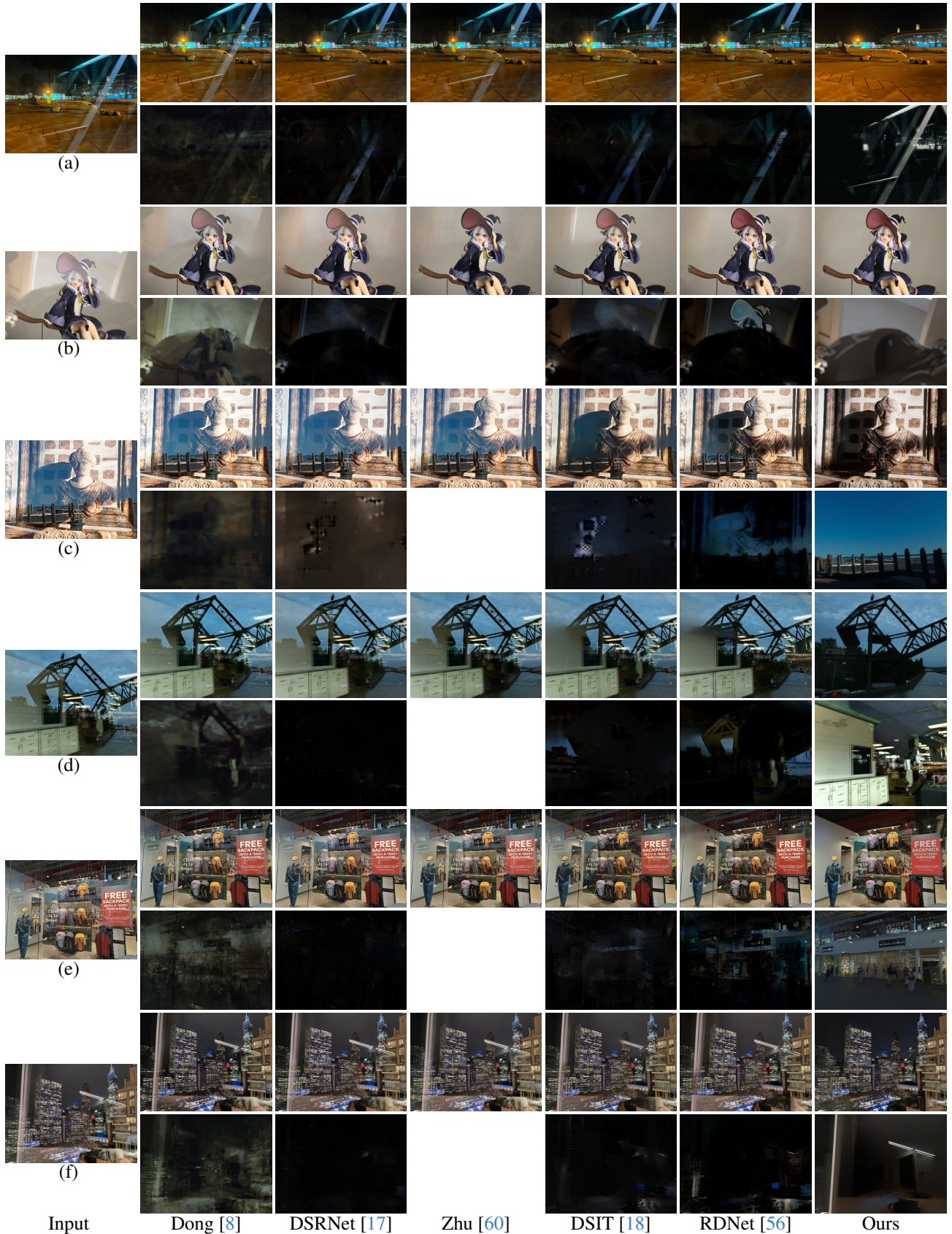


Figure 14. **More results comparison.** We compared both Transmission and Reflection of a given image with state-of-the-art methods. (a) (b) from [15]; (c) (d) from [21]; (e) (f) from our smartphone captures.